Geophysical Journal International

Geophys. J. Int. (2024) **236,** 456–469
Advance Access publication 2023 November 03
GJI Gravity, Geodesy and Tides

https://doi.org/10.1093/gji/ggad437

Combined monthly GRACE-FO gravity fields for a Global Gravity-based Groundwater Product

U. Meyer [1], M. Lasser [1], C. Dahle,[2] C. Förste,[2] S. Behzadpour,[3,*] I. Koch[4] and A. Jäggi[1]

[1] *Astronomical Institute, University of Bern,* 3012 *Bern, Switzerland. E-mail: ulrich.meyer@aiub.unibe.ch*
[2] *GFZ German Research Centre for Geosciences,* 14473 *Potsdam, Germany*
[3] *Graz University of Technology, Institut für Geodäsie,* 8010 *Graz, Austria*
[4] *Leibniz University Hannover, Institut für Erdmessung,* 30167 *Hannover, Germany*

Accepted 2023 November 2. Received 2023 May 15; in original form 2023 October 27

SUMMARY

The Combination Service for Time-variable Gravity fields (COST-G) operationally provides combinations of monthly Earth gravity field models derived from observations of the microwave ranging instrument of the GRACE Follow-on (GRACE-FO) satellite mission, applying the quality control and combination methodology originally developed by the Horizon 2020 project European Gravity Service for Improved Emergency Management for the data of the GRACE satellites. In the frame of the follow-up Horizon 2020 project Global Gravity-based Groundwater Product (G3P), the GRACE-FO combination is used to derive global grids of groundwater storage anomalies. To meet the user requirements and achieve optimal signal-to-noise ratio, the combination has been further developed and extended to incorporate:

- new time-series based on the alternative accelerometer transplant product generated in the frame of the project by the Institute of Geodesy at the Graz University of Technology, which specifically improves the estimation of the C_{30} coefficient and also reduces the noise at medium to short wavelengths, and
- the new time-series AIUB–GRACE-FO–RL02 of monthly GRACE-FO gravity fields, which is derived at the Astronomical Institute of the University of Bern by applying empirical noise modelling techniques.

The COST-G quality control confirms the consistency of the contributing GRACE-FO time-series concerning the signal amplitude of seasonal hydrology in large river basins and the secular mass change in polar regions, but it also indicates rather diverse noise characteristics. The difference in the noise levels is taken into account in the combination process by relative weights derived by variance component estimation on the solution level. The weights are expected to be inverse proportional to the noise levels of the individual gravity field solutions. However, this expectation is violated when applying the weighting scheme as developed for the GRACE combination. The reason is found in the high-order coefficients of the gravity field, which are poorly determined from the low–low range-rate observations due to the observation geometry and suffer from aliasing due to the malfunctioning accelerometer onboard one of the GRACE-FO satellites. Hence, for the final G3P-combination a revised weighting scheme is applied where the gravity field coefficients beyond order 60 are excluded from the determination of the weights.

The quality of the combined gravity fields is assessed by comparison of the noise content and the signal-to-noise ratio with the individual time-series. Independent validation is provided by the COST-G validation centre at the GFZ German Research Centre for Geosciences, where orbit fits of the low-flying Gravity and steady-state Ocean Circulation Explorer satellite are performed that confirm the high quality of the combined GRACE-FO gravity fields. By the end of the G3P project, the new combination scheme is implemented by COST-G as the

*Now at: Department of Civil, Environmental and Geomatic Engineering, ETH Zürich, Switzerland.

new COST-G–GRACE-FO–RL02 and continued to be used for the operational GRACE-FO combination.

Key words: Global change from geodesy; Satellite gravity; Time variable gravity; Glaciology; Hydrology.

1 INTRODUCTION

The Combination Service for Time-variable Gravity fields (COST-G) is a product centre of the International Gravity Field Service of the International Association of Geodesy. COST-G started operations in 2019 July (Jäggi *et al.* 2020). It collects the time-series of monthly gravity fields provided by its associated analysis centres (ACs) and partner ACs and provides robust and quality controlled combined products. Due to the diverse and independent analysis strategies applied by the individual ACs, analysis noise of the different time-series is reduced in the combination (Meyer *et al.* 2019). The COST-G quality control and combination is performed by the analysis centre coordinator (ACC) at the Astronomical Institute of the University of Bern (AIUB).

COST-G was originally set up for the combination of the monthly gravity fields of the GRACE mission (2002–2017, Tapley *et al.* 2004), but soon extended to the combination of monthly gravity fields derived from the high–low satellite tracking observations of the Swarm satellites (Teixeira da Encarnacao *et al.* 2016). COST-G was further extended to operationally combine the monthly gravity field solutions of the GRACE-FO mission in the frame of the Horizon 2020 project Global Gravity-based Groundwater Product (G3P, Güntner *et al.* 2020). The G3P-consortium moreover provided consistently generated global grids for the compartments surface water, soil moisture, snow cover, and glacial ice to derive global groundwater storage (GWS) anomalies (Güntner *et al.* 2023) from the terrestrial water storage (TWS) anomalies routinely computed from the COST-G combined monthly gravity fields.

This paper focuses on the comparison of the operational GRACE-FO combination, which is largely based on the processes originally developed for the GRACE monthly gravity fields in the frame of the Horizon 2020 project European Gravity Service for Improved Emergency Management (EGSIEM, Jäggi *et al.* 2019), with a newly developed alternative G3P-combination, taking into account alternative GRACE-FO products generated in the frame of the G3P-project. The G3P-combination is also based on a revised weighting scheme, which is in better agreement with the noise assessment of the individual time-series. Consequently, the G3P-combination outperforms the operational combination in terms of the noise assessment.

The operational GRACE-FO combination started in 2020 October. In Section 2, the time-series contributing to the combination are shortly introduced, and the impact of the accelerometer transplant product (ACT) on the individual time-series and the combination is quantified. After harmonization of all contributions, COST-G performs quality control of the individual time-series to ensure unbiased signal content of the combined products (Section 4). The monthly gravity fields are then combined by applying variance component estimation (VCE) on the solution level (Jean *et al.* 2018). The different noise levels of the individual monthly contributions are taken into account in the combination process by the relative weights (Section 3). The combined monthly gravity fields are validated internally by noise assessment over the oceans and by comparisons to the individual time-series (Section 5.1). They stand out by their favourable signal-to-noise ratio, as demonstrated by significance tests for the secular and seasonal signal content (Section 5.2). Independent validation of the individual and combined time-series is performed by the COST-G validation centre (VC) at the GFZ German Research Centre for Geosciences (GFZ), where the monthly gravity fields are used for precise orbit determination (POD) of the Gravity and steady-state Ocean Circulation Explorer (GOCE) satellite (Rummel *et al.* 2011).

The COST-G combined gravity fields are provided in three product lines, dedicated to different groups of users:

(i) Level-2 (L2) products: original spherical harmonic (SH) coefficients of the combined solutions (Meyer *et al.* 2020b).
(ii) Level-2b (L2b) products: post-processed SH coefficients (Dahle & Murböck 2020).
(iii) Level-3 (L3) products: post-processed grids or time-series of mass variations in pre-defined areas for oceanographic (Dobslaw *et al.* 2020b), hydrological (Boergens *et al.* 2020b) or glaciological applications (Sasgen *et al.* 2020b).

L2 products are disseminated via the International Centre for Global Earth Models (ICGEM,[1] Ince *et al.* 2019), L2b and L3 products are generated by the COST-G Level-3 product centre (L3C) at GFZ and disseminated via the Gravity Information Service (GravIS[2]). In the case of the G3P project the main output of the GRACE/GRACE-FO combination are the global grids of TWS-anomalies, including also uncertainty information (Boergens *et al.* 2020a), and the corresponding grids of GWS-anomalies, which are also available via GravIS, together with the compartments used for the reduction.

Currently, the following satellite-specific combinations are provided by COST-G:

(i) A complete time-series of monthly gravity fields COST-G–GRACE–RL01 (Meyer *et al.* 2020a) based on re-processed solutions derived from the GPS and *K*-band data of the dedicated gravimetric satellite mission GRACE (Tapley *et al.* 2004).
(ii) Monthly gravity fields of reduced spatial resolution (Teixeira da Encarnacao *et al.* 2019) based on the analysis of the orbits of the three satellites of ESA's magnetic field mission Swarm (Friis-Christensen *et al.* 2008) that are operationally provided on a quarterly schedule.
(iii) Monthly gravity fields COST-G–GRACE-FO–RL01-OP (Meyer *et al.* 2020b) derived from the microwave tracking system (MWI), that is, the GPS and *K*-band observations of GRACE-FO (Kornfeld *et al.* 2019; Landerer *et al.* 2020), which are also provided operationally with a latency of about two months (after the end of the respective month).

With the end of the G3P project a general switch of the COST-G operational combination scheme and a recombination of the GRACE-FO L2 time-series have been performed, which now is available as COST-G–GRACE-FO–RL02.

[1] http://icgem.gfz-potsdam.de/series
[2] http://gravis.gfz-potsdam.de/home

COST-G heavily relies on the infrastructure created and further developed in the frame of the Horizon 2020 projects EGSIEM and G3P. The Swarm combinations are generated with support of the Swarm Data, Innovation and Science Cluster (DISC, Teixeira da Encarnacao *et al.* 2020).

2 INPUT TIME-SERIES

COST-G is combining unconstrained monthly gravity fields in an SH representation. Monthly GRACE-FO gravity fields considered for the operational combination COST-G–GRACE-FO–RL01–OP are provided by the COST-G GRACE ACs GFZ (Dahle *et al.* 2019), the Centre National d'tudes Spatiales/Groupe de Recherche de Géodésie Spatiale (CNES/GRGS, Lemoine *et al.* 2007), the Institute of Geodesy at the Graz University of Technology (TUG, Kvas *et al.* 2019), AIUB (Meyer *et al.* 2016), the new COST-G GRACE-FO AC at the Leibniz University Hannover (LUH, Koch 2021), and the COST-G partner ACs at the Jet Propulsion Laboratory (JPL, Yuan 2019), and the Center for Space Research at the University of Texas, Austin (CSR, Kang *et al.* 2020).

COST-G–GRACE-FO–RL01–OP and the alternative G3P-combination are based on GPS data (or kinematic orbits derived thereof) and range-rate data of the MWI. To this date, no data of the Laser Ranging Interferometer (Sheard *et al.* 2012; Flechtner *et al.* 2016; Abich *et al.* 2019) is taken into account for the combination. In detail, the following GRACE-FO time-series are combined:

(i) AIUB–GRACE-FO operational (Lasser *et al.* 2020b) for the operational COST-G combination, or AIUB–GRACE-FO–RL02 for the G3P GRACE-FO combination,
(ii) GFZ–RL06 (GRACE-FO, Dahle *et al.* 2018) for the operational COST-G combination, or GFZ–G3P for the G3P GRACE-FO combination,
(iii) GRGS–RL05[3] unconstrained solution,
(iv) ITSG-Grace_operational_n96[4],
(v) LUH–GRACE-FO-2020 (Koch 2020),
(vi) CSR–RL06 (GRACE-FO 2019a), and
(vii) JPL–RL06 (GRACE-FO 2019b).

GFZ–G3P is an internal G3P product, all other time-series but the GRGS contribution are identical to the official releases, truncated at the common maximum degree of 90 for comparison and combination. While the official GRGS–RL05 is based on a truncated eigenvalue decomposition of combined GRACE-FO/SLR normal equations, the solutions taken into account for the COST-G or G3P GRACE-FO combinations are derived of the unconstrained GRACE-FO normal equations only.

In contrast to COST-G–RACE–RL01, the operational COST-G–GRACE-FO–RL01-OP is not based on reprocessed, standardized time-series, but on the operational products of the individual ACs provided to COST-G with short latency (i.e. within 2 months after the end of the monthly observation period). The processing strategies and background force models applied by the individual ACs may be adapted at any time, to always represent the most recent state-of-the-art in terms of the still rapidly developing insights into GRACE-FO data analysis.

[3] https://grace.obs-mip.fr/variable-models-grace-lageos/grace-solutions-release-05
[4] https://www.tugraz.at/institute/ifg/downloads/gravity-field-models/itsg-grace2018/

2.1 Alternative accelerometer transplant products

Accelerometers on both GRACE-FO satellites measure the surface forces acting on the satellites, for example, atmospheric drag or radiation pressure. The knowledge of the surface forces is necessary to separate the gravitational from the non-gravitational forces in the gravity field recovery process. However, on GRACE-D the accelerometer is malfunctioning since 2018 June and the non-conservative forces have to be modelled by an ACT-product (Bandikova *et al.* 2019) derived from the observations onboard GRACE-C. The official ACT-product is generated by JPL in the frame of the GRACE-FO Science Data System (SDS) and used in the operational RL06 products of CSR, GFZ and JPL, but four of the seven time-series contributing to the COST-G combination, namely AIUB, GRGS, ITSG and LUH, make use of an alternative ACT-product generated by TUG in the frame of the G3P project. In contrast to the SDS-ACT,[5] the G3P-ACT relies on scaled analytical force models for the low-frequency variations (Behzadpour *et al.* 2021).

For the sake of comparison, versions of the AIUB (RL01), GFZ, ITSG and LUH time-series were generated for both types of ACT-products, and test combinations of these subgroups of time-series were performed to assess the impact of the alternative ACT on the individual GRACE-FO time-series and on the combination. The time period where alternative gravity fields are available for all four time-series covers 2018 July–2021 June (in 2018 June both accelerometers were still working properly and no ACT-product has thus been generated). In case of the AIUB time-series, the monthly gravity fields based on the SDS-ACT had to be generated with a slightly modified parametrization (estimation of a full instead of a diagonal accelerometer scale factor matrix) to achieve optimal results.

The largest impact of the alternative ACT-product is found for the C_{30}-coefficient, which is important, for example, for the interpretation of ice mass change in polar regions (Loomis *et al.* 2020). C_{30} is heavily impacted by an oscillation with approximately 320 d period when based on the SDS-ACT (Fig. 1, top), as is obvious from the direct comparison to the C_{30}-values derived from independent analysis of Satellite Laser Ranging (SLR). In contrast the C_{30}-values derived based on the G3P-ACT (Fig. 1, bottom) show the expected annual variations, and also the amplitude fits very well to the SLR reference[6]. The improvement in C_{30} is in line with the evaluation by Behzadpour *et al.* (2021) based on the ITSG (TUG) time-series alone.

In the spatial domain, the artefact in the C_{30}-coefficient causes the horizontal 'zonation' typical for the zonal coefficients, in this case with three zero crossings (at the equator and at $\pm 60^\circ$ latitude), which is clearly visible in Fig. 2 (left) where the non-secular, non-seasonal geoid variations of GFZ's 2021 November gravity field based on the SDS-ACT are shown, while in the corresponding gravity field based on G3P-ACT (Fig. 2, right) the zonation has vanished.

In Fig. 3, the noise of the different time-series is assessed in the spectral domain in terms of difference degree amplitudes by comparison to the independent GOCO06s (Kvas *et al.* 2021) gravity field (including the time-variable part of GOCO06s). All individual

[5] Recently, revised RL06.1 time-series have become available from the SDS-ACs, which make use of a new ACT-product from JPL with properties very much comparable to the G3P-ACT; the SDS-RL06.1 time-series are used in the COST-G-GRACE-FO-RL02 combination.
[6] ftp://isdcftp.gfz-potsdam.de/grace-fo/DOCUMENTS/TECHNICAL_NOTES/TN-14_C30_C20_SLR_GSFC.txt

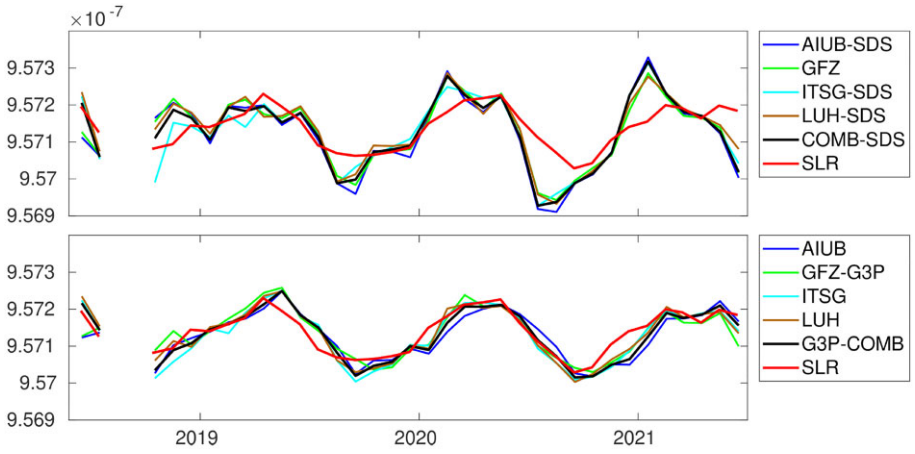

Figure 1. Estimates of C_{30} based on the SDS-ACT (top) and the G3P-ACT (bottom); SLR for reference.

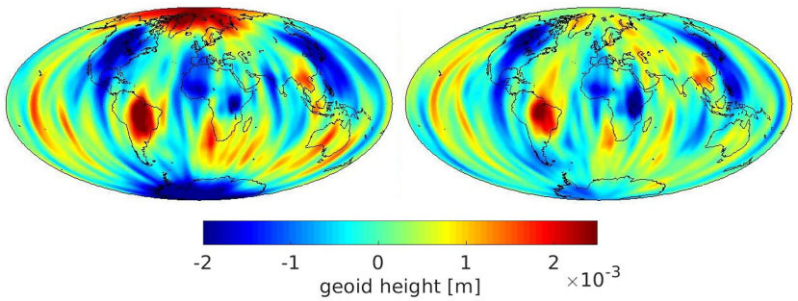

Figure 2. Non-secular, non-seasonal geoid variations of the GFZ monthly gravity field 2021 November based on either SDS-ACT (left) or G3P-ACT (right).

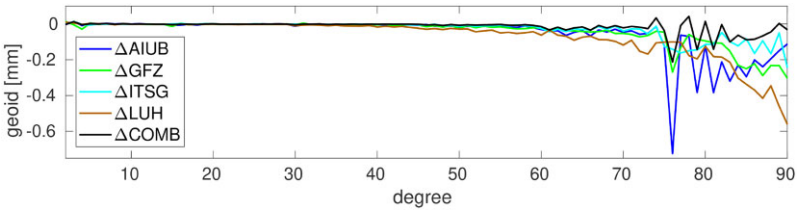

Figure 3. Change of difference degree amplitudes of individual and combined time-series with respect to GOCO06s (including time variations) when using G3P-ACT instead of SDS-ACT; negative values indicate noise reduction.

time-series based on the G3P-ACT reveal reduced noise levels in the medium to high degrees when compared to their respective counterparts based on the SDS-ACT. When comparing the combination of the four time-series based on G3P-ACT with the combination of the four time-series based on SDS-ACT, the improvement is largely reduced. We conclude that the noise induced by the SDS-ACT in the medium to high degrees is mainly of a stochastic nature and is already effectively reduced by the combination. Improvements in low-degree coefficients are masked by the extrapolation error of the time-variable signal component of GOCO06s, but are rather small anyway.

In Fig. 4, the monthly noise of the combined time-series based on G3P-ACT is assessed in terms of the non-seasonal, non-secular variability over ocean areas (see Section 4.3), and the differences in the individual and the combined time-series due to the use of either SDS- or G3P-ACT are provided. For all four individual time-series, improvements in case of using the G3P-ACT are visible in most of the monthly solutions. The degradation in the 2018 June AIUB gravity field is caused by the adaption of the parametrization (see above) which is infavourable in the presence of real accelerometer observations from both satellites. The large improvement in case of the monthly LUH gravity fields of 2021 June most probably is due to a processing artefact. The combination only profits in a few months from the improvements in the individual time-series, and the effect is rather small. The limited improvement in the combination is in line with the evaluation in the spectral domain (Fig. 3).

Fig. 5 exemplarily depicts the spatial distribution of the non-secular, non-seasonal variability in terms of the root mean square (RMS) per grid cell over all monthly gravity fields of the GFZ time-series based either on the SDS-ACT (left) or on the G3P-ACT (right). The variations are transformed to equivalent water height (EWH) to focus on the medium-degree coefficients (high-degree noise and signal is attenuated by the application of a 400 km Gauss filter). The noise level can be assessed by the RMS over ocean areas, where little short-term variability due to hydrological signal is expected. The reduction in noise related to the improved ACT-product is mainly visible in polar regions, where the impact of the C_{30}-coefficient (see Fig. 2) is most pronounced and where medium-

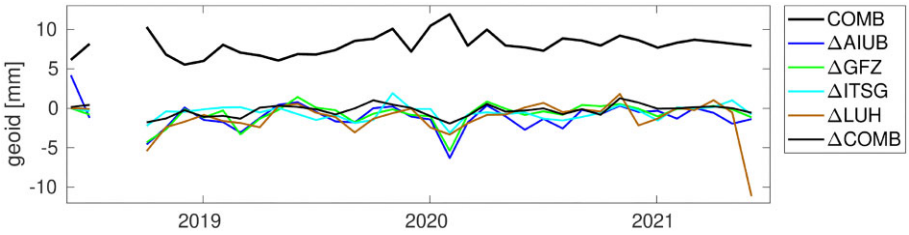

Figure 4. Noise assessment of the combined time-series and impact of the choice of ACT on the individual time-series (G3P-ACT solutions – SDS-ACT solutions; negative values indicate noise reduction).

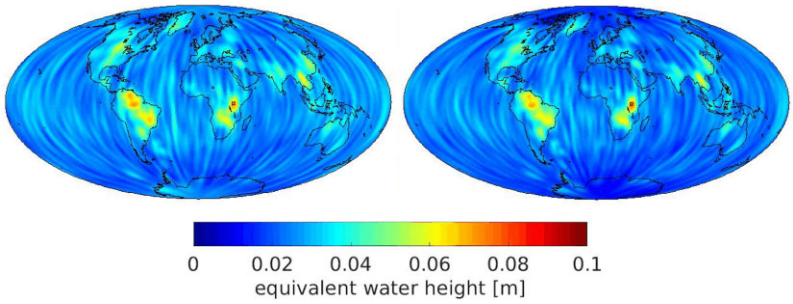

Figure 5. Non-secular, non-seasonal EWH variability (smoothed by a 400 km Gauss filter) of the GFZ time-series based on either SDS-ACT (left) or G3P-ACT (right).

to high-degree coefficients generally profit from the dense ground-track spacing. A slight improvement is also visible over mid- to low-latitude oceans.

3 COMBINATION

The main task of COST-G is the monthly combination of the individual gravity field solutions. A combination on normal equation level would be feasible, at least for the ACs providing monthly normal equations, but due to unrealistic stochastic models provided with most of the normal equations, this would require the use of empirical scaling factors (Meyer *et al.* 2019). For the reason of simplicity, in order to also take the partner ACs into account which do not provide normal equations, and to avoid any empirical treatment that would make the interpretation of differences difficult, the operational COST-G and the G3P GRACE-FO combination are performed on solution level, at the cost of ignoring correlations between gravity field and orbit or instrument parameters.

3.1 RL01 weighting scheme

Relative weights are derived iteratively by VCE on the solution level (Jean *et al.* 2018). Prior to combination, the SH coefficients are scaled to a common Earth radius R and gravity constant times mass of the Earth GM, and the handling of the permanent tide affecting C_{20} is harmonized. All ACs apply the linear mean pole model (Petit & Luzum 2010,v1.2), therefore no adaption of the C_{21} and S_{21} coefficients is necessary. Degree 1 coefficients, which are included in the GRGS time-series, are neglected in the combination and set to zero in the combined product. The Earth's flattening coefficient C_{20} is neglected in the derivation of the relative weights due to its rather large scatter, which is not representative for the overall quality of the monthly solutions, but is included in the L2-combination.[7] All other SH coefficients up to degree 90 enter the VCE with equal *a priori* weights. Error estimates in the individual gravity fields are ignored because most of the ACs provide formal errors that strongly depend on their processing strategy and parametrization. They are very diverse and do not reflect the actual quality of the gravity field coefficients.

The determined weights are applied equally to all coefficients of the monthly gravity field. In case of equal signal content of all individual gravity fields, the weights are expected to be inversely proportional to the mean noise content of all coefficients of the corresponding gravity field. In Fig. 6 (top), the relative weights for the GRACE-FO time-series contributing to the COST-G combination are shown. With few exceptions, the relative weights of the individual time-series are rather stable. In 2018 October and 2019 February, the GRGS and ITSG monthly solutions are degraded, because they refer to the data of the corresponding month only, while all other ACs apply the time-windows as defined by the GRACE-FO SDS for their monthly solutions, which deviate in these two cases from the strictly monthly schedule due to data gaps.

The noise assessment for the different time-series and the COST-G combination is shown in Fig. 6 (bottom). It is based on the non-secular, non-seasonal variability over ocean areas, where only very little short-term variations are to be expected, for example, due to errors in the atmosphere and ocean de-aliasing (AOD) products (see Section 4.3). Corresponding to the weights, the increased noise of GRGS and ITSG in 2018 October and 2019 February is visible, a period of increased noise in 2020 January/February affects most of the time-series (the reason for this is unclear). Otherwise, the noise levels of the different time-series are rather stable over the whole

[7] in the L2b- and L3-products C_{20} is replaced by values derived from combined GRACE-FO and SLR analyses.

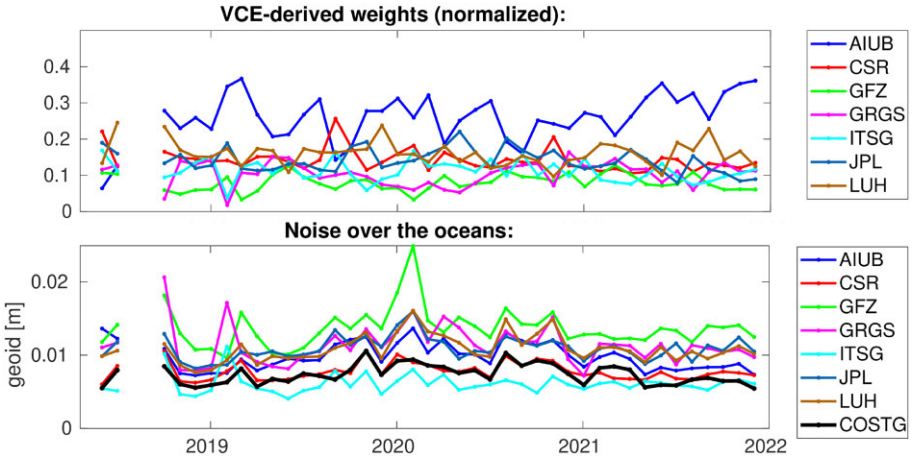

Figure 6. Monthly weights used for the COST-G combination (top), and noise assessment, that is, monthly RMS of non-secular, non-seasonal variability over the oceans (bottom).

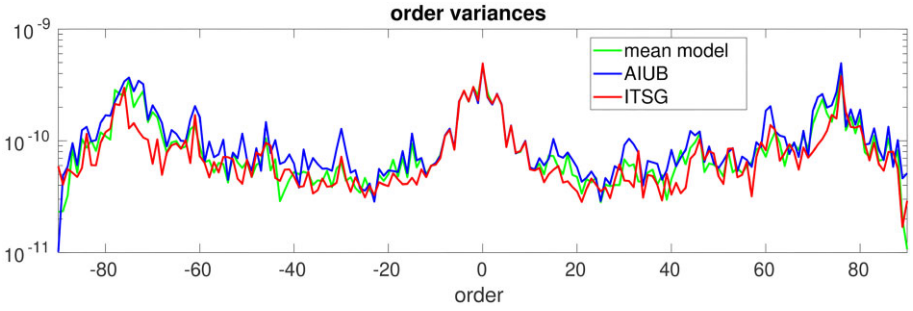

Figure 7. Order amplitudes of annual variations, fitted to the individual gravity field coefficients.

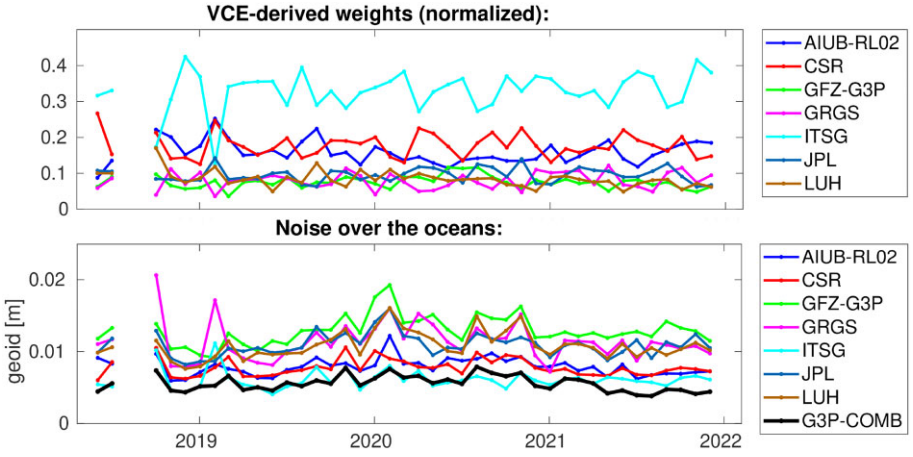

Figure 8. Alternative weights of G3P GRACE-FO combination (top) based on coefficients of orders ≤60, and corresponding noise assessment (bottom).

GRACE-FO mission period and are in agreement with the noise assessment in the spectral domain in Fig. 13.

Comparing relative weights and noise levels, the consistent assessment in case of GRGS and GFZ, with rather high noise and low weights, and in case of JPL and LUH, with medium weights and noise levels, is in accordance with our expectation. Surprisingly, the CSR and ITSG time-series, which feature very favourable noise levels, get only moderate VCE weights. The opposite is true for the AIUB contribution, with low to medium noise level, but high weights. The latter behaviour was already observed in case of the GRACE combination in the frame of the EGSIEM project (Jäggi *et al.* 2019), where a consistent background modelling by all EGSIEM ACs was emphasized. It was explained by Jean *et al.* (2018) by the special effort made at AIUB to provide unbiased solutions, which due to their closeness to the arithmetic mean of all time-series get high VCE weights.

The discrepancy between the noise assessment and the VCE weights of the ITSG time-series was also observed, to a lesser extent, by Jean *et al.* (2018) in case of the GRACE combinations in the frame of the EGSIEM project. It has been explained by the empirical noise modelling approach of ITSG, which is very successful in suppressing noise, especially in the high-degree and -order coefficients,

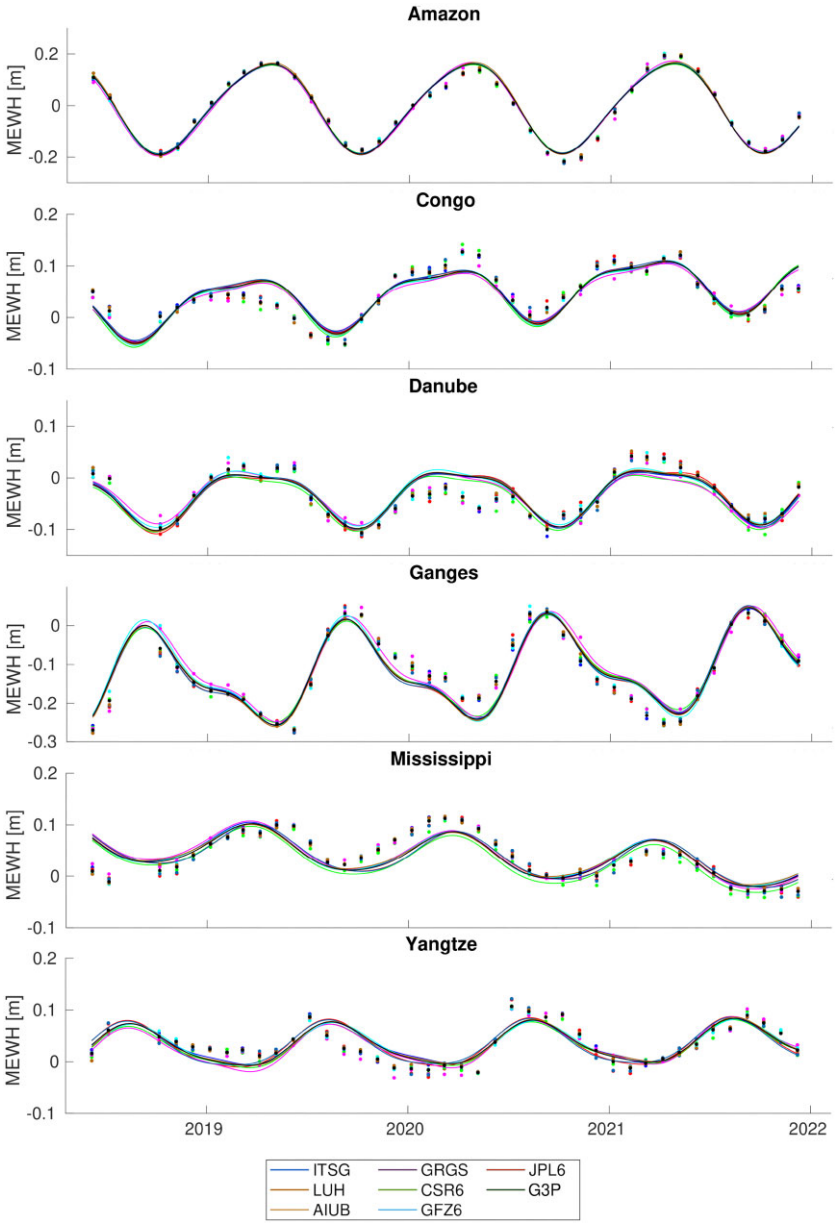

Figure 9. Time-series of MEWH for selected river basins. Dots indicate monthly estimates, continuous curves represent the signal models fitted to the individual time-series. All monthly solutions were smoothed by a 400 km Gauss filter.

which suffer from systematic variations. In Fig. 7, order amplitudes are shown for coefficient-wise amplitudes of annual variations, fitted to the time-series of the individual coefficients of the monthly AIUB and ITSG gravity fields and of monthly mean gravity fields, averaged over all ACs. The order amplitudes were computed corresponding to the commonly shown degree amplitudes. They provide an assessment of the order-wise seasonal signal content. Below order 12 all time-series agree very well and the order amplitudes can be assumed to represent true signal content. Peaks round the resonant orders 15, 31, 46, 61 and 76 are artefacts due to aliasing, possibly caused by spectral leakage of seasonal signal from low-degree coefficients. While AIUB is in very good agreement with the monthly mean gravity fields beyond order 60, ITSG managed to reduce the signal aliasing at high orders. As a consequence, ITSG is punished by VCE for applying a noise modelling strategy that is different from the majority of the GRACE-FO ACs, irrespective of most probably being closer to reality, while AIUB is getting high weights in the combination due to being close to the mean.

3.2 G3P weighting scheme

Due to the fact that the error information in the different time-series is very diverse and not calibrated in most cases, it is ignored in the COST-G combination approach and all coefficients contribute equally to the derivation of the weights. Consequently, the weights are dominated by the high-degree coefficients by sheer number. Experiments, where the impact of the high-degree coefficients of the individual gravity fields on their relative weights was reduced by application of a Gauss filter (Wahr *et al.* 1998), did not yield satisfactory results (not shown). Instead, we focus on the role of the high-order coefficients, which due to the along-track observation geometry of the *K*-band range-rate observations, in conjunction

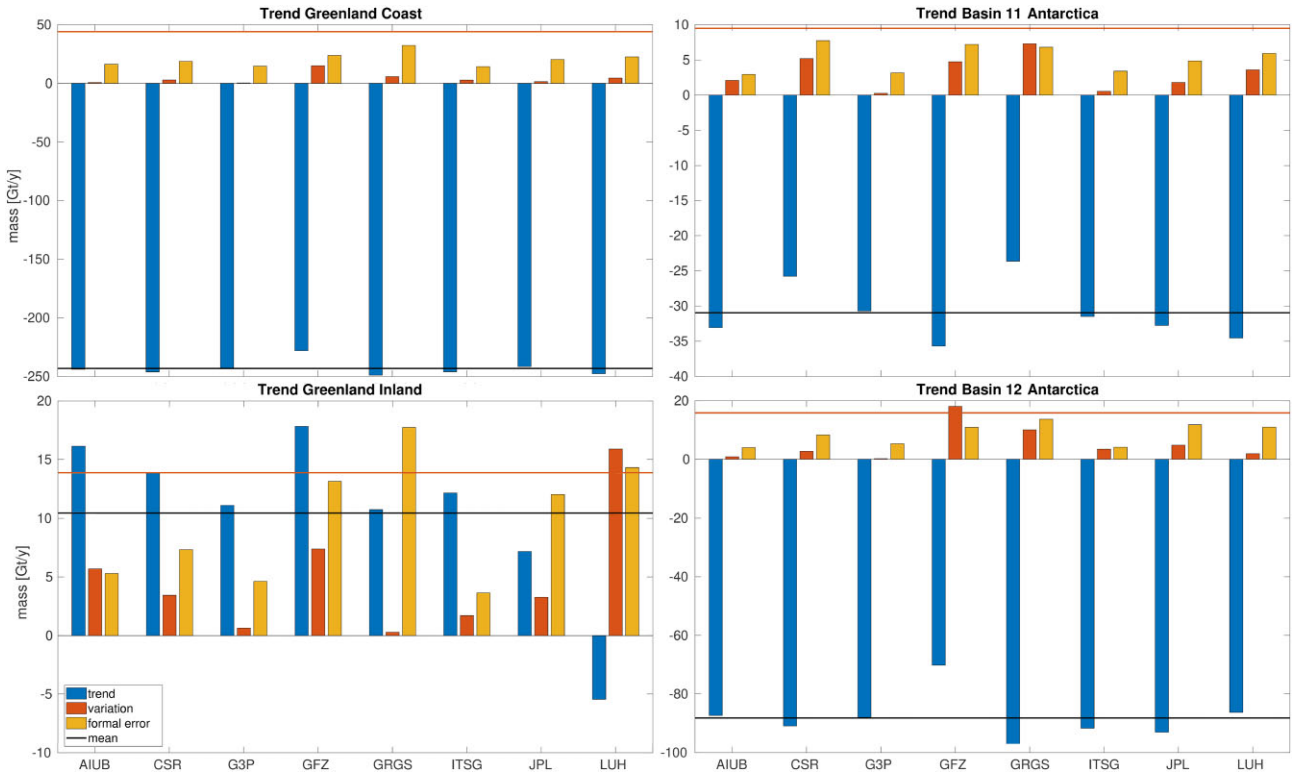

Figure 10. Annual mass loss (blue) in Greenland (top left: coastal regions and bottom left: inland ice shield) and Antarctica (top right: basin 11 and bottom right: basin 12, compare to Fig. 11). The deviation (red) from the arithmetic mean of all time-series (black line) and the formal error of the estimation of the mass trend (orange) are provided for the assessment of significance. The red line indicates three times the formal error of the combination.

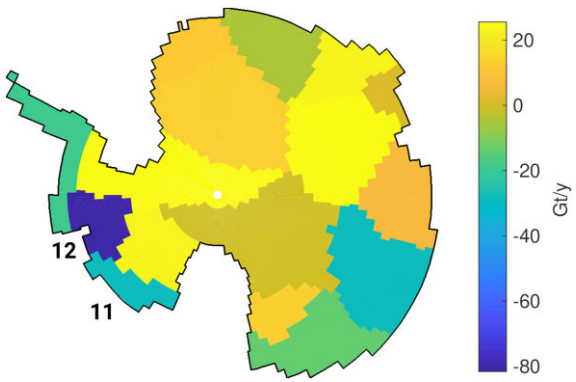

Figure 11. Mean mass trends in glacial basins in Antarctica. Further studied are basins 11 and 12 along the west coast.

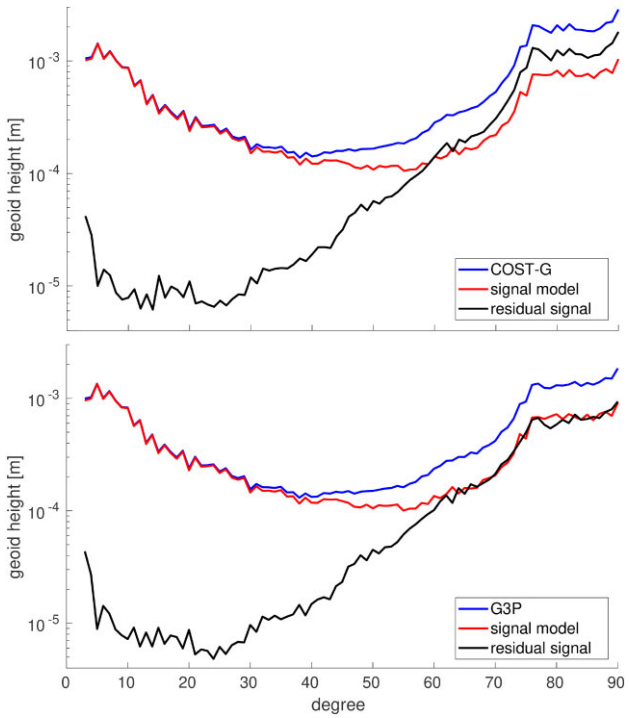

Figure 12. Mean difference degree amplitudes of the monthly gravity fields and the signal model with respect to the static reference GOCO06S, and residuals of the signal model with respect to the monthly averages (top COST-G combination and bottom G3P GRACE-FO combination).

with the near polar orbits of the GRACE-FO satellites, are poorly determined (Weigelt *et al.* 2013). Consequently, the high-order coefficients are 'easy victims' to spectral leakage from low-degree coefficients and are contaminated by rather strong seasonal variations (Jean *et al.* 2018, compare also Fig. 7).

We apply a very simple order-specific filter by limiting the maximum order of the coefficients considered for the derivation of the weights to 60. The limit of 60 was determined empirically, based on the time period covered by the G3P results. As opposed to directly using the very diverse error information for weighting, this approach allows for a consistent treatment of all time-series and is well suited for an operational environment. The impact on the weights (Fig. 8, top) is drastic. ITSG now takes the lead for most of the monthly combinations, followed by CSR and AIUB. The

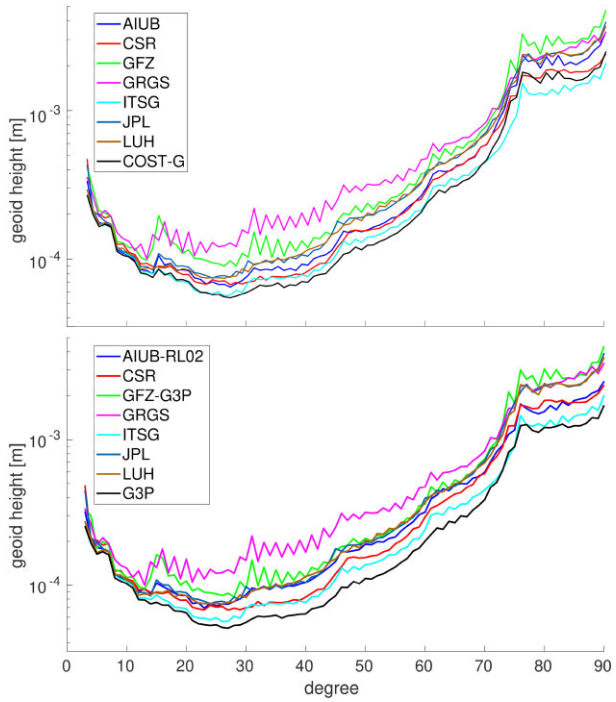

Figure 13. Mean difference degree amplitudes with respect to the signal model (top COST-G combination and bottom G3P GRACE-FO combination).

weights therefore are much more consistent with the results of the noise assessment (Fig. 8, bottom, and Fig. 13). As a direct result, the G3P GRACE-FO combination now outperforms also the best individual time-series (ITSG) in most of the months, especially in 2021.

4 QUALITY CONTROL

COST-G is performing quality control to ensure comparable signal content of all individual contributions. The quality control is based on the fit and comparison of a deterministic signal model to time variations of EWH in river basins (from the model Total Runoff Integration Pathways, TRIP),[8] or to mass variations in polar regions. The deterministic signal model consists of a constant mean, secular variations, as well as annual and semi-annual periodic variations.

In case of the comparison of seasonal variations of hydrological origin in large river basins, the monthly solutions are smoothed by a 400 km Gauss filter (Wahr *et al.* 1998), transformed to 1° grids, and the monthly mean EWH (MEWH) per basin is computed by summation over all grid cells within the river basin, weighted according to cell size by the cosine of the cell's midpoint latitude. In case of the comparison of mass trends in glacial basins along the coasts of Greenland or Antarctica, no filter is applied to avoid filter attenuation due to signal leakage into the oceans.

The longer the time-series of monthly solutions, the more reliable is the fit of the signal models, and the more meaningful is the inter-comparison of the signal content of the individual time-series. The G3P GRACE-FO time-series spans the period 2018 June to 2021 December with gaps only due to missing observation data in 2018 August and September. In case of the evaluation of smoothed gravity fields in large river basins, the period of more than three years of data is sufficient for a meaningful comparison. In case of non-smoothed mass trends, the evaluation turned out to provide reliable results only for the larger glacial basins.

4.1 Amplitude of seasonal variations

Fig. 9 shows monthly estimates (dots) of MEWH for selected river basins and the deterministic signal models (lines) fitted to the individual time-series and the G3P GRACE-FO combination. While the fit of our simplistic signal model is very good for the large Amazon basin, in other river basins it obviously cannot follow all excursions of the monthly EWH estimates in the full extent. Nevertheless, the differences between the signal models are rather small, even for the river basins with strong semi-annual variations, for example, Congo, Danube or Ganges. The amplitudes of the periodic annual component of the signal models of the individual time-series and the COST-G operational and G3P GRACE-FO combinations for selected river basins, as well as the scatter (RMS) with respect to the mean amplitudes of all ACs in the 50 largest river basins of the world, the mean bias per AC and its standard deviation (STD) are compiled in Table 1. The maximum systematic deviation in the annual amplitude is 3.7 mm in case of CSR, the largest scatter (with respect of the respective average amplitude per basin) is also observed for CSR with an RMS of 7.0 mm. While all biases but the very small ITSG bias can be determined significantly from the data according to an F-test (e.g. Snedecor & Cochran 1989), in general the AC-specific biases are much smaller than their STDs. From the comparison of the seasonal hydrological variations and considering the small (compared to the scatter) systematic deviations, we conclude that none of the time-series suffers from relevant signal attenuation, as could originate from intentional or accidental regularization (Meyer *et al.* 2015).

4.2 Mass trends in polar regions

Secular mass trends in polar regions are studied for Greenland and the west coast of Antarctica, where strong ice mass loss has been observed (e.g. Wouters *et al.* 2014; Tapley *et al.* 2019; Velicogna *et al.* 2020; Sasgen *et al.* 2020a). Mass change is computed from EWH by multiplication with the density of water. Again, the same type of deterministic signal model is used, but this time we focus on the trend component. No attempt is made to correct for glacial isostatic adjustment, to account for snow cover or to quantify leakage effects. The only purpose of the assessment is the inter-comparison of the time-series to detect outliers in signal content.

In Fig. 10, the annual mass change in Greenland (left) for all individual GRACE-FO time-series and the G3P GRACE-FO combination is compared. To assess the deviations, the differences to the arithmetic mean of the mass trends of all time-series and the formal errors of the trends, originating from the fit of the signal model, are provided as well. Due to the small sample size of only seven time-series we base our outlier detection criterion on the formal errors of the trends. Deviations from average that are larger than three times the formal error of the combination are rated outliers.

The main Greenland mass loss is concentrated at low altitudes along the coasts, while on the inland ice sheet a small mass gain can be observed (Harig *et al.* 2012), which is commonly attributed to increased precipitation related to the warming of the atmosphere (Holube *et al.* 2022). Along the coasts the trend estimates of all time-series agree well (Fig. 10, top left). In case of the inland ice

[8] http://hydro.iis.u-tokyo.ac.jp/~taikan/TRIPDATA/TRIPDATA.html

Table 1. Amplitude of annual variations in centimeter EWH for selected river basins and overall statistical information. The scatter and mean bias refer to the arithmetic mean annual amplitude of all time-series per basin and are computed from the 50 largest river basins.

basin	AIUB	AIUB–RL02	CSR	GFZ	GFZ–G3P	GRGS	ITSG	JPL	LUH	COST-G	G3P
Amazon	17.2	17.2	17.0	16.5	16.9	17.5	17.3	17.1	17.5	17.2	17.2
Congo	5.1	5.0	5.2	5.0	5.2	4.6	5.2	5.1	5.1	5.1	5.1
Danube	5.1	5.1	5.2	5.1	5.0	4.8	5.1	5.2	5.2	5.1	5.1
Ganges	11.1	10.9	11.1	11.1	10.8	11.3	11.6	11.1	11.3	11.2	11.1
Mississippi	4.2	4.2	4.2	4.4	4.2	4.2	4.1	4.2	3.9	4.1	4.1
Yangtze	3.7	3.8	4.5	4.1	3.9	4.1	4.0	4.3	4.0	4.0	4.0
Scatter (RMS)	0.39	0.28	0.70	0.49	0.35	0.32	0.26	0.60	0.28	0.21	0.18
Mean bias	−0.22	−0.15	0.37	0.16	−0.18	−0.13	−0.02	0.30	−0.10	−0.11	−0.08
STD of bias	0.33	0.24	0.60	0.46	0.31	0.30	0.26	0.53	0.26	0.18	0.16

shield all time-series but LUH reveal small mass gain (Fig. 10, bottom left). The difference of the LUH trend estimate from the average trend of all time-series is larger than three times the formal error of the combination and consequently is rated as outlier.

We extend the trend estimation to glacial basins of Antarctica (Fig. 11) and again evaluate the individual time-series and the G3P GRACE-FO combination. The mass loss is strongest at the west coast, where we take a closer look at the two glacial basins 11, and 12 (Fig. 10, right). In the small basin 11 (Bakutis Coast to Cape Colbeck) with moderate mass loss, all time-series agree within the limits of the outlier criterion (Fig. 10, top right). In basin 12 (Eights and Walgreen Coast), where the thinning and breaking loose of the shelf ice in the Amundsen See is leading to an increased flow rate of near coastal glaciers (Jacobs *et al.* 2012) and consequently to a large mass loss, the trend estimate of the GFZ time-series violates the outlier criterion (Fig. 10, bottom right).

A direct comparison of the estimated mass trends is provided in Table 2, which includes also both versions of the combination and the AIUB and GFZ time-series. The spread among the trend estimates of the different AC's time-series for individual basins can reach $20 - 30\,\mathrm{Gt\,y^{-1}}$. Rather large deviations in the GFZ time-series may be related to problematic C_{21}, S_{21}-coefficients (Dahle *et al.* 2019) that affect mass change estimates in polar regions. Consequently, these coefficients are replaced for the GFZ solutions in the generation of the L2b- and L3-products. The only remaining outlier is the trend estimate of LUH in inland Greenland, where the scatter of all time-series is rather large compared to the small mass gain observed. Since LUH is not conspicuous in any of the other regions and since the trend estimates of the unfiltered time-series in small basins is still weak due to the short time period of only three year, we refrain from excluding LUH from the combination. The scatter is efficiently reduced in the COST-G and G3P GRACE-FO combinations, where the agreement is at the level of $0.4 - 3.6\,\mathrm{Gt\,y^{-1}}$. We conclude that the new weighting scheme has no significant impact on the signal content, while it efficiently reduces the noise.

4.3 Noise assessment

In addition to the comparisons of the signal content, also noise assessment is performed as part of the COST-G quality control. 'Noise' is assessed on the basis of monthly residuals with respect to a deterministic signal model, which is adjusted to the unweighted monthly averages of the gravity fields of all time-series of the time-period 2018 June–2021 December. The model consists of mean, bias, secular, annual and semi-annual periodic variations and is fitted to each SH coefficient separately. The monthly residuals with respect to this signal model are evaluated in the spectral domain (Fig. 12). While these residuals contain also unmodelled signal, at medium to high SH degree they are dominated by noise. The same is true in the spatial domain for ocean areas and large deserts, where little hydrological variability is expected (see Section 5.1).

In Fig. 12, the descending part (approximate degrees 3–40) of the mean differences of the monthly average gravity fields and the signal model with respect to the static part of the independent multimission gravity field GOCO06s (Kvas *et al.* 2021) indicate that the degree range is dominated by time-variable signal content. The rising difference degree amplitudes of the monthly average gravity fields beyond degree 40 have to be attributed mainly to noise. The rise in the difference degree amplitudes of the signal model beyond degree 60 is caused by seasonal and secular components in the noise. Up to approximately degree 30, the difference degree amplitudes of the residuals of the average monthly gravity fields with respect to the signal model are mainly caused by non-modelled signal content. The large residuals in degree 3 are related to accelerometer artefacts (as discussed in Section 2.1). The rise of the residuals beyond degree 30 is attributed to noise and is further used to characterize the noise levels of the different time-series. In the comparison of the G3P GRACE-FO and the COST-G combination the lower noise content at high degrees stands out. Note that the power of the secular and seasonal signal content, as represented by the signal model, is almost unchanged in the G3P GRACE-FO combination.

The noise assessment of the individual time-series, based on the signal model discussed above, is provided in Fig. 13. It indicates rather large noise content in the medium degree range for the unconstrained GRGS and the GFZ time-series, whereas ITSG, CSR and AIUB have the lowest noise levels. In the comparison of the operational COST-G and the G3P GRACE-FO combination the lower noise of the G3P GRACE-FO combination stands out, which in contrast to the COST-G combination outperforms the individual time-series also in the highest degrees. Concerning the individual time-series, only the GFZ- and AIUB-solutions differ. In case of GFZ–G3P, a slight reduction of noise in the medium to high degrees is visible. In case of AIUB–RL02, the noise reduction is limited to high degrees, whereas in the medium degrees a small degradation is visible, which needs to be further investigated.

In the frame of the COST-G quality control, the noise assessment of the individual time-series or monthly solutions is only performed to give feedback to the COST-G ACs. High noise levels are no argument against inclusion of a time-series in the combination, because the different noise levels are taken into account in the combination process by the relative weights determined by VCE (see Section 3).

Table 2. Mass trend estimates in Gt y^{-1}.

Basin	AIUB	AIUB–RL02	CSR	GFZ	GFZ–G3P	GRGS	ITSG	JPL	LUH	COST-G	G3P
Greenland coast	−237.7	−243.9	−246.1	−248.6	−228.1	−248.9	−246.0	−241.6	−247.7	−244.9	−242.8
Greenland inland	15.3	16.1	13.9	19.2	17.8	10.7	12.2	7.2	−5.5	10.7	11.1
Antarctic basin 11	−32.1	−33.1	−25.8	−38.2	−35.7	−23.7	−31.5	−32.8	−34.6	−31.1	−30.7
Antarctic basin 12	−83.4	−87.3	−91.0	−77.6	−70.1	−98.3	−91.7	−93.1	−86.3	−86.7	−88.0

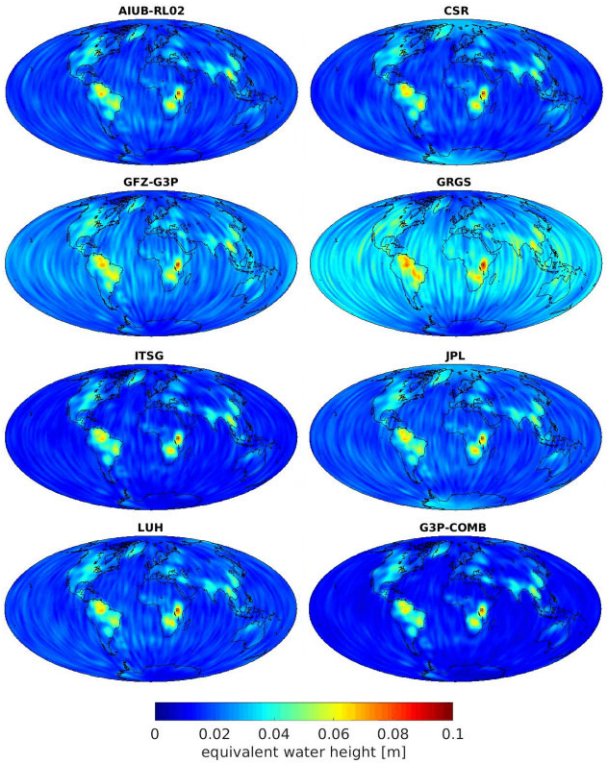

Figure 14. RMS of non-secular, non-seasonal EWH variations in the spatial domain, smoothed by a 400 km Gauss filter.

5 INTERNAL VALIDATION

5.1 Noise level

For the assessment of the noise level of the combined monthly gravity fields, the same tools are used as outlined in Section 4.3 for the COST-G quality control and are also applied in Section 3 for the consistency check of the weights determined by VCE. In addition to the noise assessment in Fig. 8 (bottom), we provide the spatial representation of the residual variability in global plots (Fig. 14). Over the continents, the variability is caused mainly by non-seasonal hydrological mass change and represents interesting signal that has to be preserved in the combination process. Over the oceans, where little short-term hydrological signal has to be expected, the remaining variability serves to assess the noise level of the different time-series.

The noise assessment of the individual time-series is in agreement with Fig. 13, where the residual variability was addressed in the spectral domain. A degradation over polar regions in case of the CSR and JPL time-series is related to the SDS-ACT used in these two time-series (see Section 2.1). The ITSG time-series and G3P GRACE-FO combination reveal the smallest variability over the oceans (Table 3).

Table 3. Ocean RMS of the residual EWH variability [mm] over the oceans.

AIUB	CSR	GFZ	GRGS	ITSG	JPL	LUH	G3P
2.7	3.1	3.8	5.8	2.3	3.0	2.7	2.3

5.2 Signal content

As long as no signal attenuation by unintentional regularization has escaped the COST-G quality control, the signal content of the combined gravity fields does not differ from that of the individual time-series. Therefore the combined time-series was already included in the comparison of hydrological variations within selected river basins (Fig. 9 and Table 1). As may be expected, the combined gravity fields yield results close to the mean amplitudes of all time-series. The same is true for the mass trends derived for polar regions (Table 2).

What is gained by the combination is an improved signal-to-noise ratio, which is illustrated by the results of statistical *F*-tests of the estimated trends and annual variations per SH coefficient. In Fig. 15, the cumulative distribution functions of the trends (left) and annual variations (right) per SH coefficient are provided for the G3P GRACE-FO combination (Fig. 15, bottom), and for comparison also for the GFZ–G3P time-series (Fig. 15, top). In case of the combined time-series, significant trends and annual variations can be determined for more coefficients than in case of the individual AC's time-series, here exemplified by GFZ–G3P. Spectral leakage into high-degree coefficients, as indicated by vertical strings of significant coefficients of the same order up to high degrees, is also reduced in the combined time-series. We therefore conclude that due to the improved signal-to-noise ratio, time-variable signal can be recovered at smaller spatial scales from the combined time-series than from the individual time-series.

6 EXTERNAL VALIDATION

The COST-G VCs perform independent validation of the individual and the combined time-series that goes beyond the consistency checks and noise assessment provided above.

6.1 Orbit fits

The Earth's gravity field is the major force acting on a satellite. In consequence, POD, especially of Low Earth Orbiters (LEOs), relies on a precise gravity field model. Vice versa, fitting orbits to satellite observations is a quality indicator for the applied force model including the gravity field. Therefore, the COST-G monthly gravity fields are here evaluated via POD of the GOCE satellite mission (Drinkwater *et al.* 2007). This particular LEO, which was in orbit from 2009 till 2013, had a very low orbital altitude of about 255 km and thus showed a very high sensitivity to the Earth's gravity field. For the purpose of evaluation, 3-D kinematic orbit positions of reprocessed orbit products GO_CONS_SST_PKI_2I (Bock *et al.* 2011) are used as pseudo-observations in a dynamic orbit adjustment. Here, the gravitational forces are modelled according

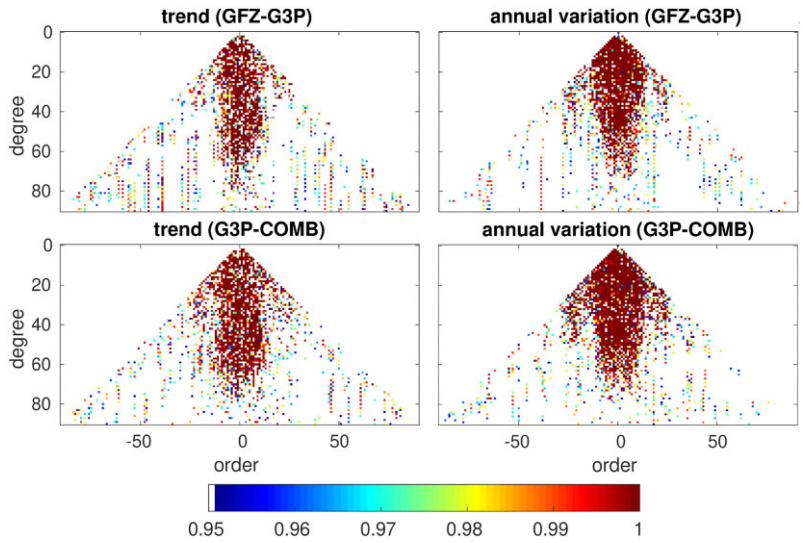

Figure 15. Cumulative distribution function of trends (left) and annual variations (right) indicating the significance per SH coefficient of the GFZ-G3P (top) and G3P GRACE-FO combination (bottom) time-series, as determined by a statistical *F*-test.

Table 4. GOCE orbit fit results (3-D RMS values [cm] of the orbit fit residuals, i.e. mean values from the involved arcs in question, bold numbers indicate best results).

Month	March			April			June			December		
Year	2019	2020	2021	2019	2020	2021	2019	2020	2021	2019	2020	2021
AIUB	6.68	7.58	7.90	6.80	7.87	8.13	6.70	7.75	7.88	7.40	8.27	8.11
AIUB–RL02	6.37	7.58	7.76	6.92	7.32	7.88	6.24	8.05	7.71	6.63	7.75	8.47
GFZ	8.40	8.60	8.30	8.78	8.36	8.52	7.22	8.61	9.68	7.64	8.88	10.09
GFZ–G3P	8.28	7.94	8.39	7.41	8.27	8.66	7.42	8.18	9.06	7.61	8.25	9.53
GRGS	7.05	8.04	8.27	6.90	8.64	8.59	6.81	8.55	10.17	7.72	7.87	8.38
ITSG	5.94	6.95	7.11	**5.93**	6.69	**7.08**	**5.68**	**6.33**	**6.77**	**6.17**	6.95	7.36
LUH	8.12	8.01	8.40	6.81	8.11	8.67	8.04	8.35	9.24	7.41	8.57	8.13
CSR	6.59	7.76	7.71	6.69	7.07	8.30	6.80	7.58	9.18	7.67	7.83	7.94
JPL	7.85	7.70	8.70	7.89	8.20	8.69	7.29	8.32	9.21	7.60	8.04	8.66
COST-G	6.42	7.10	7.27	6.36	7.06	7.84	6.40	7.36	7.62	6.94	7.51	7.57
G3P	**5.92**	**6.76**	**6.79**	5.99	**6.55**	7.30	5.85	6.68	6.86	6.38	**6.77**	**7.21**

to the different monthly gravity field models under consideration, whereas the non-gravitational accelerations are described by the GOCE common-mode acceleration data. In order to not suffer from large omission errors of the time-variable GRACE-FO solutions, whose maximum SH degree and order is not larger than 96, all monthly models to be evaluated are filled up to degree and order 240 with the SH coefficients of the static satellite-only model GO_CONS_GCF_2_DIR_R6 (Förste *et al.* 2019).

In the context of this investigation, a setup of 1252 GOCE orbits with 30 hr arc length from the entire GOCE mission period has been established for this and future orbit fit evaluations. The parameters as here adjusted in the dynamic orbit determination are the six orbital elements at the beginning of each arc, and the biases of the three common-mode acceleration axes (along-track, cross-track and radial) per arc. Furthermore, the common-mode accelerometer scale factors are fixed to 1.0 in all three axes. The evaluation results are the 3-D RMS values of the orbit fit residuals (i.e. the mean values from the involved arcs in question).

The orbit tests were done for GRACE-FO models of the months March, April, June and December out of the years 2019, 2020 and 2021 for individual GRACE-FO time-series as well as for the COST-G and the G3P GRACE-FO combinations. Each of these monthly models was tested in all available GOCE arcs for the respective calendar months out of the years 2009–2013 (March 110 arcs, April 121 arcs, June 110 arcs and December 117 arcs). In this context, the permanent tide system of all included solutions has been harmonized into tide free and in case of GRGS the unconstrained solutions were used.

The 3-D RMS values of the mean residuals over all arcs are given in Table 4. One must have in mind that the mission periods of GOCE (2009–2013) and GRACE-FO (since 2018) are non-overlapping. Therefore, the orbit fit experiment is not suited to evaluate the GRACE-FO temporal gravity variations in an absolute sense. But one can assume hat the model uncertainty associated with the striding ahead temporal gravity variations is the same for all time-series. Hence, the observed differences in the fit are caused by the different noise behaviour.

All monthly gravity fields to be evaluated were truncated at the same SH degree of 90 for comparability, but otherwise not filtered. The orbit fit results for the 12 example months clearly indicate quality differences between the individual models, the spread of the results reaches 20 per cent in terms of the 3-D orbit fit. Among the time-series of the individual ACs the ITSG monthly gravity fields generally provide the closest orbit fit, outperformed only by the G3P GRACE-FO combination in 6/12 months. The validation

also confirms the improvement of GFZ–G3P over the operational GFZ time-series in 9/12 months, where AIUB–RL02 outperforms the operational AIUB time-series in 8/12 cases. The orbit validation therefore confirms the results of the internal noise assessment.

7 CONCLUSIONS

We have introduced the operational COST-G GRACE-FO combination and the alternative GRACE-FO combination developed in the frame of the G3P project. The time-series of monthly gravity fields contributing to the combinations and both combined time-series are compared in terms of their signal and noise content in the spectral and the spatial domain. Special attention is paid to the role of the ACT product used for the generation of the monthly gravity fields and the weighting scheme applied in the combination.

The G3P-ACT mainly affects the C_{30} gravity field coefficient, where it drastically reduces the artefacts present in the C_{30} based on the original SDS-ACT. The noise content in the medium- to high-degree coefficients is also slightly reduced, but the effect on the combination in this degree range is limited due to the stochastic nature of the noise which is already efficiently reduced by the combination process.

The weights which are derived by VCE on the solution level in the operational COST-G combination are deteriorated by coloured noise in the high-order gravity field coefficients. The omission of the high-order coefficients, which are poorly defined from GRACE-FO range-rate observations, in the derivation of the relative weights improves the consistency between the weights and the noise assessment of the individual time-series, and in consequence leads to significantly improved combined solutions.

The G3P GRACE-FO combination stands out by its low noise content and consequently improved signal-to-noise ratio, mainly at medium to high SH degrees, which could be confirmed by orbit fits of the low-flying GOCE satellite, where the G3P GRACE-FO combination outperforms the best of the individual AC's time-series (ITSG) in 50 per cent, and the operational COST-G combination in 100 per cent of the test cases.

As a consequence of the positive evaluation, the operational COST-G combination will be switched to the G3P GRACE-FO combination scheme with the end of the G3P project and the existing COST-G GRACE-FO combined time-series is reprocessed as RL02, also taking into account the GRACE-FO SDS RL06.1 time-series based on the new, improved SDS-ACT. COST-G–GRACE-FO–RL02 is made available by ICGEM, the corresponding L3-products are distributed via GravIS.

It should be noted that currently many of the GRACE-FO ACs work on empirical noise modelling strategies. Consequently, it may be expected that future gravity field releases will feature not only a general noise reduction, as illustrated most prominently by the ITSG time-series, but also calibrated error estimates which will allow for a further iteration of the COST-G weighting scheme, and presumably a combination on the normal equation level.

ACKNOWLEDGMENTS

This project has received funding from the European Union's Horizon 2020 research and innovation programme under grant agreement no. 870353. The views expressed herein can in no way be taken to reflect the official opinion of the European Union. The research was also supported by the International Space Science Institute (ISSI) in Bern, through ISSI International Team project 424 (International Combination Service for Time-variable Gravity Field Solutions). UM performed the quality control, combinations and internal validation of the combined time-series and compiled the manuscript; SB provided the G3P-ACT; ML, CD and IK provided specific time-series for the experiments on the G3P-ACT; CF performed the GOCE orbits tests and provided Section 6.1 and AJ provided supervision of the project. The authors are not aware of any competing interests.

DATA AVAILABILITY

Combined monthly GRACE-FO gravity fields in SH coefficients (L2-products, Meyer *et al.* 2020b) are available from the ICGEM, http://icgem.gfz-potsdam.de/series.

REFERENCES

Abich, K. *et al.*, 2019. In-orbit performance of the GRACE Follow-On laser ranging interferometer, *Phys. Rev. Lett.,* **123**(3), 031101 , doi:10.1103/PhysRevLett.123.031101.

Bandikova, T., Mccullough, C., Kruizinga, G. L., Save, H. & Christophe, B., 2019. GRACE accelerometer data transplant, *Adv. Space Res.,* **64,** 623–633.

Behzadpour, S., Mayer-Gürr, T. & Krauss, S., 2021. GRACE Follow-On accelerometer data recovery, *J. geophys. Res.—Solid Earth,* **126,** e2020JB021297 , doi:10.1029/2020JB021297.

Bock, H., Jäggi, A., Meyer, U., Visser, P., van den IJssel, J., van Helleputte, T., Heinze, M. & Hugentobler, U., 2011. GPS-derived orbits for the GOCE satellite, *J. Geod.,* **85,** 807–818.

Boergens, E., Dobslaw, H., Dill, R., Thomas, M., Dahle, C., Murböck, M. & Flechtner, F., 2020a. Modelling spatial covariances for terrestrial water storage variations verified with synthetic GRACE-FO data, *Int. J. Geomath.,* **11**(24) , doi:10.1007/s13137-020-00160-0.

Boergens, E., Dobslaw, H. & Dill, R., 2020b. COST-G GravIS RL01 continental water storage anomalies. V. 0004 (Data set), *GFZ Data Services* , doi:10.5880/COST-G.GRAVIS_01_L3_TWS.

Dahle, C., Flechtner, F., Murböck, M., Michalak, G., Neumayer, H., Abrykosov, O., Reinhold, A. & König, R., 2018. GRACE geopotential GSM coefficients GFZ RL06 (Data set), *GFZ Data Services* , doi:10.5880/gfz.grace_06_gsm.

Dahle, C. *et al.*, 2019. The GFZ GRACE RL06 monthly gravity field time series: processing details and quality assessment, *Remote Sens.,* **11**(18), 2116 , doi:10.3390/rs11182116.

Dahle, C. & Murböck, M., 2020. Post-processed GRACE/GRACE-FO geopotential GSM coefficients COST-G RL01 (Level-2B Product). V. 0002 (Data set), *GFZ Data Services* , doi:10.5880/COST-G.GRAVIS_01_L2B.

Dobslaw, H., Boergens, E. & Dill, R., 2020b. COST-G GravIS RL01 ocean bottom pressure anomalies. V. 0004 (Data set), *GFZ Data Services* , doi:10.5880/COST-G.GRAVIS_01_L3_OBP.

Drinkwater, M., Haagmans, R., Muzzi, D., Popescu, A., Floberghagen, R., Kern, M. & Fehringer, M., 2007. The GOCE gravity mission: ESA's first core explorer, in *Proceedings 3rd GOCE User Workshop,* pp. 1–8, European Space Agency, Noordwijk, ESA SP-627.

Flechtner, F., Neumayer, K.H., Dahle, C., Dobslaw, H., Fagiolini, E., Raimondo, J.C. & Güntner, A., 2016. What can be expected from the GRACE-FO laser ranging interferometer for Earth science applications?, *Surv. Geophys.,* **37,** 453–470.

Förste, C., Abrykosov, O., Bruinsma, S., Dahle, C., König, R. & Lemoine, J.-M., 2019. ESA's Release 6 GOCE gravity field model by means of the direct approach based on improved filtering of the reprocessed gradients of the entire mission (GO_CONS_GCF_2_DIR_R6), *GFZ Data Services* , doi:10.5880/ICGEM.2019.004.

Friis-Christensen, E., Lühr, H., Knudsen, D. & Haagmans, R., 2008. Swarm—an earth observation mission investigating geospace, *Adv. Space Res.,* **41,** 210–216.

GRACE-FO, 2019a. GRACE-FO monthly geopotential spherical harmonics CSR release 6.0 (Data set), *NASA Jet Propulsion Laboratory (JPL), NASA Physical Oceanography DAAC* , doi:10.5067/GFL20-MC060.

GRACE-FO, 2019b. GRACE-FO monthly geopotential spherical harmonics JPL release 6.0 (Data set), *NASA Jet Propulsion Laboratory (JPL), NASA Physical Oceanography DAAC* , doi:10.5067/GFL20-MJ060.

Güntner, A. *et al.*, 2020. *Towards an Operational Copernicus Service: a Global Gravity-based Groundwater Product (G3P),* H079-06, AGU 2020 Fall Meeting (Online). https://agu.confex.com/agu/fm20/meetingapp.cgi/Paper/745984 accessed 17/11/2023.

Güntner, A., Sharifi, E., Ruz Vargas, C. & Kidd, R., 2023. *G3P Product Report,* https://cordis.europa.eu/project/id/870353 accessed 17/11/2023.

Harig, C. & Simons, F. J., 2012. Mapping Greenland's mass loss in space and time, *PNAS,* **109**(49), 19934–19937.

Holube, K. M., Zolles, T. & Borm, A., 2022. Sources of uncertainty in Greenland surface mass balance in the 21st century, *The Cryosphere,* **16,** 315–331.

Ince, E.S., Barthelmes, F., Reißland, S., Elger, K., Förste, C., Flechtner, F. & Schuh, H., 2019. ICGEM – 15 years of successful collection and distribution of global gravitational models, associated services, and future plans, *Earth Syst. Sci. Data,* **11,** 647–674.

Jacobs, A., Jenkins, A., Hellmer, H., Giulivi, C., Nitsche, F., Huber, B. & Guerero, R., 2012. The Amundsen Sea and the Antarctic Ice Sheet, *Oceanography,* **25**(3), 154–163.

Jäggi, A. *et al.*, 2019. European Gravity Service for Improved Emergency Management (EGSIEM) - from concept to implementation, *Geophys. J. Int.,* **218**(3), 1572–1590.

Jäggi, A. *et al.*, 2019. *International Combination Service for Time-Variable Gravity Fields (COST-G) - Start of Operational Phase and Future Perspectives, In: IAG Symp. Ser.,* ed. Freymueller, J., Springer, Berlin, Heidelberg , doi:10.1007/1345_2020_109.

Jean, Y., Meyer, U. & Jäggi, A., 2018. Combination of GRACE monthly gravity field solutions from different processing strategies, *J. Geod.,* **92,** 1313–1328.

Kang, Z., Bettadpur, S., Nagel, P., Save, H., Poole, S. & Pie, N., 2020. GRACE-FO precise orbit determination and gravity recovery, *J. Geod.,* **94**(9), 85 , doi:10.1007/s00190-020-01414-3.

Koch, I., 2020. *LUH-GRACE-FO-2020 (Data set),* LUIS , doi:10.25835/0062546.

Koch, I., Duwe, M., Flury, J. & Shabanloui, A., 2021. Earth's time-variable gravity from GRACE Follow-On K-band range-rates and pseudo-observed orbits, *Remote Sens.,* **13**(9), 1766 , doi:10.3390/rs13091766.

Kornfeld, R.P., Arnold, B.W., Gross, M.A., Dahya, N.T., Klipstein, W.M., Gath, P.F. & Bettadpur, S., 2019. GRACE-FO: The Gravity Recovery and Climate Experiment Follow-On Mission, *J. Spacecraft Rockets,* **56**(3), 931–951.

Kvas, A., Behzadpour, S., Ellmer, M., Klinger, B., Strasser, S., Zehentner, N. & Mayer-Gürr, T., 2019. ITSG-Grace2018: Overview and evaluation of a new GRACE-only gravity field time series, *J. geophys. Res.—Solid Earth,* **124,** 9332–9344.

Kvas, A. *et al.*, 2021. GOCO06s – a satellite-only global gravity field model, *Earth Syst. Sci. Data,* **13,** 99–118.

Landerer, F.W. *et al.*, 2020. Extending the global mass change data record: GRACE follow-on instrument and science data performance, *Geophys. Res. Lett.,* **47,** e2020GL088306 , doi:10.1029/2020GL088306.

Lasser, M., Meyer, U., Arnold, D. & Jäggi, A., 2020. AIUB-GRACE-FO-operational – Operational GRACE Follow-On monthly gravity field solutions (Data set), *GFZ Data Services*. doi: 10.5880/icgem.2020.001.

Lemoine, J.-M., Bruinsma, S., Loyer, S., Biancale, R., Marty, J.-C., Perosanz, F., Balmino & G, 2007. Temporal gravity field models inferred from GRACE data, *Adv. Space Res.,* **39,** 1620–1629 . doi:10.1016/j.asr.2007.03.062.

Loomis, B.D., Rachlin, K.E., Wiese, D.N., Landerer, F.W. & Luthcke, S.B., 2020. Replacing GRACE/GRACE-FO C30 with satellite laser ranging: impacts on Antarctic ice sheet mass change, *Geophys. Res. Lett.,* **47**(3), e85488 , doi:10.1029/2019GL085488.

Meyer, U., Jäggi, A., Beutler, G., Bock & H.xi, 2015. The impact of common versus separate estimation of orbit parameters on GRACE gravity field solutions, *J. Geod.,* **89(7),** 685–696.

Meyer, U., Jäggi, A., Jean, Y. & Beutler, G., 2016. AIUB-RL02: an improved time-series of monthly gravity fields from GRACE data, *Geophys. J. Int.,* **205,** 1196–1207 , doi:10.1093/gji/ggw081.

Meyer, U., Jean, Y., Kvas, A., Dahle, C., Lemoine, J.-M. & Jäggi, A., 2019. Combination of GRACE monthly gravity fields on the normal equation level, *J. Geod.,* **93,** 1645–1658.

Meyer, U. *et al.*, 2020a. International combination service for time-variable gravity fields (COST-G) monthly GRACE series. V. 01 (Data set), *GFZ Data Services* , doi:10.5880/ICGEM.COST-G.001.

Meyer, U. *et al.*, 2020b. International combination service for time-variable gravity fields (COST-G) monthly GRACE-FO S=series. V. 01 (Data set), *GFZ Data Services* , doi:10.5880/ICGEM.COST-G.002.

Petit, G. & Luzum, B., 2010. IERS conventions, *IERS Technical Note 36, Verlag des Bundesamts für Kartographie und Geodäsie,* Frankfurt am Main.

Rummel, R., Yi, W. & Stummer, C., 2011. GOCE gravitational gradiometry, *J. Geod.,* **85,** 777–790.

Sheard, B.S., Heinzel, G., Danzmann, K., Shaddock, D.A., Klipstein, W.M. & Folkner, W.M., 2012. Intersatellite laser ranging instrument for the GRACE follow-on mission, *J. Geod.,* **86,** 1083–1095 , doi:10.1007/s00190-012-0566-3.

Sasgen, I. *et al.*, 2020a. Return to rapid ice loss in Greenland and record loss in 2019 detected by the GRACE-FO satellites, *Commun. Earth Environ.,* **1**(1), 8. doi: 10.1038/s43247-020-0010-1.

Sasgen, I., Groh, A. & Horwath, M., 2020b. COST-G GravIS RL01 Ice-Mass Change Products. V. 0002 (Data set), *GFZ Data Services* , doi:10.5880/COST-G.GRAVIS_01_L3_ICE.

Snedecor, G.W. & Cochrane, W.G., 1989. *Statistical Methods,* 8th edn, Iowa State University Press.

Tapley, B., Bettadpur, S., Watkins, M. & Reigber, C., 2004. The gravity recovery and climate experiment: mission overview and early results, *Geophys. Res. Lett.,* **31,** L09607 , doi:10.1029/2004GL019920.

Tapley, B.D. *et al.*, 2019. Contributions of GRACE to understanding climate change, *Nat. Clim. Change,* **9,** 358–369.

Teixeira da Encarnao, J. *et al.*, 2016. Gravity field models derived from Swarm GPS data, *Earth Planets Space,* **68**(127) , doi:10.1186/s40623-016-0499-9.

Teixeira da Encarnao, J. *et al.*, 2019. Multi-approach gravity field models from Swarm GPS data (Data set), *GFZ Data Services* , doi:10.5880/ICGEM.2019.006.

Teixeira da Encarnao, J. *et al.*, 2020. Description of the multi-approach gravity field models from Swarm GPS data, *Earth Syst. Sci. Data,* **12**(2), 1385–1417.

Velicogna, I. *et al.*, 2020. Continuity of ice sheet mass loss in Greenland and Antarctica from the GRACE and GRACE Follow-On missions, *Geophys. Res. Lett.,* **47**(8), e87291 , doi:10.1029/2020GL087291.

Wahr, J., Molenaar, M. & Bryan, F., 1998. Time variability of the Earth's gravity field: hydrological and oceanic effects and their possible detection using GRACE, *J. geophys. Res.,* **103**(B12), 30205–30229.

Weigelt, M., Sneeuw, N., Schrama, E.J.O. & Visser, P.N.A.M., 2013. An improved sampling rule for mapping geopotential functions of a planet from a near polar orbit, *J. Geod.,* **87,** 127–142.

Wouters, B., Bonin, J.A., Chambers, D.P., Riva, R.E.M., Sasgen, I. & Wahr, J., 2014. GRACE, time-varying gravity, Earth system dynamics and climate change, *Rep. Prog. Phys.* , doi:10.1088/0034-4885/77/11/116801.

Yuan, D.-N., 2019. *GRACE Follow-On Level-2 Gravity Field Product User Handbook*. Jet Propulsion Laboratory, JPL D-103922, https://podaac-tools.jpl.nasa.gov/drive/files/allData/gracefo/docs/GRACE-FO_L2-UserHandbook_v1.0.pdf.